

What drives gravitational instability in nearby star-forming spirals? The impact of CO and H I velocity dispersions

Alessandro B. Romeo¹ and Keoikantse Moses Mogotsi²

¹*Department of Earth and Space Sciences, Chalmers University of Technology, SE-41296 Gothenburg, Sweden*

²*South African Astronomical Observatory, PO Box 9, Observatory, Cape Town, 7935 South Africa*

Accepted 2017 April 1. Received 2017 March 24; in original form 2017 January 9

ABSTRACT

The velocity dispersion of cold interstellar gas, σ , is one of the quantities that most radically affect the onset of gravitational instabilities in galaxy discs, and the quantity that is most drastically approximated in stability analyses. Here we analyse the stability of a large sample of nearby star-forming spirals treating molecular gas, atomic gas and stars as three distinct components, and using radial profiles of σ_{CO} and $\sigma_{\text{H I}}$ derived from HERA CO-Line Extragalactic Survey (HERACLES) and The H I Nearby Galaxy Survey (THINGS) observations. We show that the radial variations of σ_{CO} and $\sigma_{\text{H I}}$ have a weak effect on the local stability level of galaxy discs, which remains remarkably flat and well above unity, but is low enough to ensure (marginal) instability against non-axisymmetric perturbations and gas dissipation. More importantly, the radial variation of σ_{CO} has a strong impact on the size of the regions over which gravitational instabilities develop, and results in a characteristic instability scale that is one order of magnitude larger than the Toomre length of molecular gas. Disc instabilities are driven, in fact, by the self-gravity of stars at kiloparsec scales. This is true across the entire optical disc of every galaxy in the sample, with a few exceptions. In the linear phase of the disc-instability process, stars and molecular gas are strongly coupled, and it is such a coupling that ultimately triggers local gravitational collapse/fragmentation in the molecular gas.

Key words: instabilities – stars: kinematics and dynamics – ISM: kinematics and dynamics – galaxies: ISM – galaxies: kinematics and dynamics – galaxies: star formation.

1 INTRODUCTION

Gravitational instability is one of the engines behind the dynamics of disc galaxies, where it enters a variety of processes: from the formation of stars (Elmegreen 2012), globular clusters (Kruijssen 2014) and giant molecular clouds (Dobbs et al. 2014) to the formation and evolution of spiral structure (Bertin 2014) and bars (Athanasoula 2013; Sellwood 2014), including the growth of bars within bars and associated structures (Shlosman, Frank & Begelman 1989). Today, several decades after the pioneering works of Safronov (1960), Toomre (1964) and Goldreich & Lynden-Bell (1965a,b) on local disc instability, and the seminal papers by Lin & Shu (1966) and Jog & Solomon (1984a,b) on the relative contributions of stars and interstellar gas, it is widely accepted that cold gas plays an important role in the instability scenario even though it contributes little to the self-gravity of the disc. Numerous multicomponent stability analyses have also shown that the colder the gas, i.e. the lower its 1D velocity dispersion σ , the higher its impact on the onset of disc instabilities (e.g. Bertin & Romeo 1988, and

references therein; Elmegreen 1995; Jog 1996; Rafikov 2001; Kim & Ostriker 2007; Elmegreen 2011; Romeo & Falstad 2013, and references therein).

Clearly, σ is a quantity of great importance not only for the onset of gravitational instabilities in galaxy discs, but also for other dynamical processes. For example, σ is one of the most basic diagnostics of interstellar turbulence (see e.g. Elmegreen & Scalo 2004; Hennebelle & Falgarone 2012), which itself has an impact on *both* star formation (e.g. Krumholz & McKee 2005; Kraljic et al. 2014; Salim, Federrath & Kewley 2015; Semenov, Kravtsov & Gnedin 2016) and local disc instability (e.g. Elmegreen 1996; Romeo, Burkert & Agertz 2010; Shadmehri & Khajenabi 2012; Agertz, Romeo & Grisdale 2015, and references therein). Other examples and references are given by Mogotsi et al. (2016, hereafter M16).

NGC 6946 provides an eloquent example of how radically σ can affect the onset of gravitational instabilities in galaxy discs, and how drastically σ is approximated in stability analyses (Ferguson et al. 1998; Romeo & Fathi 2015). In particular, Ferguson et al. (1998) showed that if one assumes $\sigma = 6 \text{ km s}^{-1}$, the classical value motivated by Kennicutt (1989), then this galaxy turns out to be unstable up to the edge of the optical disc, while using a

* E-mail: romeo@chalmers.se

radial profile of σ derived from observations yields stability across the entire disc! Martin & Kennicutt (2001) pointed out that radial variation in σ remains controversial because such measurements demand both high angular resolution and high brightness sensitivity, requirements not met by most observations. Fortunately, recent CO and H I galaxy surveys [BIMA Survey of Nearby Galaxies (BIMA SONG), HERA CO-Line Extragalactic Survey (HERACLES) and The H I Nearby Galaxy Survey (THINGS)] have provided high-quality measurements of molecular and atomic gas kinematics, which allow deriving reliable radial profiles of σ_{CO} and $\sigma_{\text{H I}}$ (e.g. Tamburro et al. 2009; Caldú-Primo et al. 2013; Ianjamasimanana et al. 2015; Romeo & Fathi 2015; M16; Romeo & Fathi 2016; Ianjamasimanana, de Blok & Heald 2017). In particular, Romeo & Fathi (2015) analysed NGC 6946 in detail and showed that the observed radial variation of σ_{CO} has indeed a significant impact on disc instabilities.

Does the observed radial variation of σ_{CO} , or that of $\sigma_{\text{H I}}$, have a significant impact on disc instabilities even in other galaxies? If so, how does the new instability scenario differ from the classical one? To explore this important aspect of the problem, we consider a large sample of nearby star-forming spirals and use newly derived radial profiles of σ_{CO} and $\sigma_{\text{H I}}$, together with the disc instability diagnostics developed by Romeo & Falstad (2013). Such diagnostics follow from rigorous stability analyses (Romeo 1985; Bertin & Romeo 1988; Romeo 1990, 1992, 1994), and they are more general than the effective Q parameter proposed by Romeo & Wiegert (2011) and as easy to use. Using such diagnostics one can measure the local stability level of galaxy discs and the size of the regions over which gravitational instabilities develop, and one can also predict which gas or stellar component drives the instability process. This has been illustrated in a variety of applications (e.g. Genzel et al. 2014; Westfall et al. 2014; Fathi et al. 2015; Romeo & Fathi 2015; Hallenbeck et al. 2016; Inoue et al. 2016; Romeo & Fathi 2016; Williamson, Martel & Kawata 2016a,b; Fiacconi et al. 2017). In this paper, we consider not only molecular and atomic gas, but also a component that is still often disregarded when analysing the stability of spiral galaxies: the stars! The data and method are described in Section 2, the results are presented in Section 3 and discussed in Section 4, and the conclusions are drawn in Section 5.

2 DATA AND METHOD

We consider a sample of 12 nearby star-forming spirals that was previously analysed by Leroy et al. (2008, hereafter L08) and Romeo & Falstad (2013), among others: NGC 628, 2841, 3184, 3198, 3351, 3521, 3627, 4736, 5055, 5194, 6946 and 7331. These are galaxies with sensitive and spatially resolved measurements across the entire optical disc, which L08 selected from the following surveys: the BIMA SONG (Helfer et al. 2003), the HERACLES (Leroy et al. 2009), the SIRTf/Spitzer Infrared Nearby Galaxies Survey (SINGS; Kennicutt et al. 2003) and THINGS (Walter et al. 2008). We refer to L08 for a detailed description of the data and their translation into physical quantities (see their section 3).

Following Romeo & Falstad (2013), we treat all the molecular gas, atomic gas and stars as three distinct components and use the same epicyclic frequency (κ), surface densities (Σ_{CO} , $\Sigma_{\text{H I}}$ and Σ_{\star}) and stellar radial velocity dispersion (σ_{\star}) as in L08 (see their appendices A–C and E–F). However, rather than using observationally motivated values of the CO and H I 1D (line-of-sight) velocity dispersions, we use observed radial profiles of σ_{CO} and $\sigma_{\text{H I}}$, which we

describe in Section 2.1. Note two points concerning our notation:

- (i) Σ_{CO} denotes the *total* surface density of molecular hydrogen + helium gas, as traced by CO emission (our $\Sigma_{\text{CO}} = \text{L08's } \Sigma_{\text{H}_2}$).
- (ii) σ_{CO} , $\sigma_{\text{H I}}$ and σ_{\star} denote *dynamically different* quantities. To first approximation, molecular gas and atomic gas are collisional so their velocity dispersions are isotropic (see e.g. Bertin 2014). This is true even considering the effects of gas turbulence and stellar feedback (Grisdale et al. 2017). In contrast, the stellar component is collisionless and has an anisotropic velocity dispersion (see again Bertin 2014).

2.1 Radial profiles of the CO and H I velocity dispersions

To derive $\sigma_{\text{CO}}(R)$ and $\sigma_{\text{H I}}(R)$, we use Hanning-smoothed CO ($J = 2 \rightarrow 1$) data cubes from HERACLES and natural-weighted H I data cubes from THINGS, and adapt the method used by M16 to the present context. In fact, a few refinements are needed to derive reliable radial profiles of σ_{CO} and $\sigma_{\text{H I}}$ for all spirals of our sample (NGC 3521, 3627, 5194 and 7331 were not included in M16), and to ensure that the resulting $\sigma_{\text{CO}}(R)$ and $\sigma_{\text{H I}}(R)$ are fully consistent with all other radial profiles (same sampling and range as in L08). Our method is described step by step below:

- (i) We smooth the H I data to 13 arcsec to match the spatial resolution of the CO data, as in M16.
- (ii) We fit single Gaussians to the CO and H I velocity profiles, as in M16.
- (iii) We then consider the CO and the H I fits *separately*. We impose a peak amplitude cut-off equal to four times the root-mean-square level of noise, and retain only those pixels where the peak amplitude is greater than this cut-off value. M16 imposed, instead, a more restrictive condition, namely that *both* the CO *and* the H I peak amplitudes should be greater than the cut-off value above. Our way of processing the data is consistent with the method used by L08, who derived $\Sigma_{\text{CO}}(R)$ and $\Sigma_{\text{H I}}(R)$ *independently of each other*.
- (iv) We also impose a velocity dispersion cut-off equal to the typical velocity resolution of the data (5.2 km s⁻¹ for CO, and 2.6 or 5.2 km s⁻¹ for H I), and retain only those pixels where the velocity dispersion is greater than this cut-off value. Our approach differs from that followed by M16 as highlighted in item (iii).
- (v) We further impose a cut-off of 2.6 km s⁻¹ on the fitted velocity dispersion uncertainties, and remove all pixels with uncertainties larger than this cut-off value. Such a condition was not imposed by M16, but is useful because it reduces beam smearing and other projection effects significantly. These effects are greatest in the central regions of highly inclined galaxies, where they cause artificial profile broadening and asymmetric profile shapes, especially when the velocity resolution of the data is low (e.g. Teuben 2002; Caldú-Primo et al. 2013). Our condition removes most of those velocity profiles, and allows a more accurate determination of velocity dispersions using simple Gaussian fits.
- (vi) We mask out further spurious emission in the CO and H I data using the HERACLES and THINGS moment-0 maps.
- (vii) Finally, we compute $\sigma_{\text{CO}}(R)$ and $\sigma_{\text{H I}}(R)$ from the CO and H I velocity dispersion maps derived above, averaging azimuthally over 10-arcsec-wide tilted rings. We estimate the error bars of $\sigma_{\text{CO}}(R)$ and $\sigma_{\text{H I}}(R)$ using the traditional formula

$$\Delta X = \text{RMS}/\sqrt{n}, \quad (1)$$

where ΔX is the uncertainty in a quantity X averaged over a tilted ring, RMS is the root-mean-square scatter within the tilted ring and n is the number of resolution elements in the ring (i.e. the

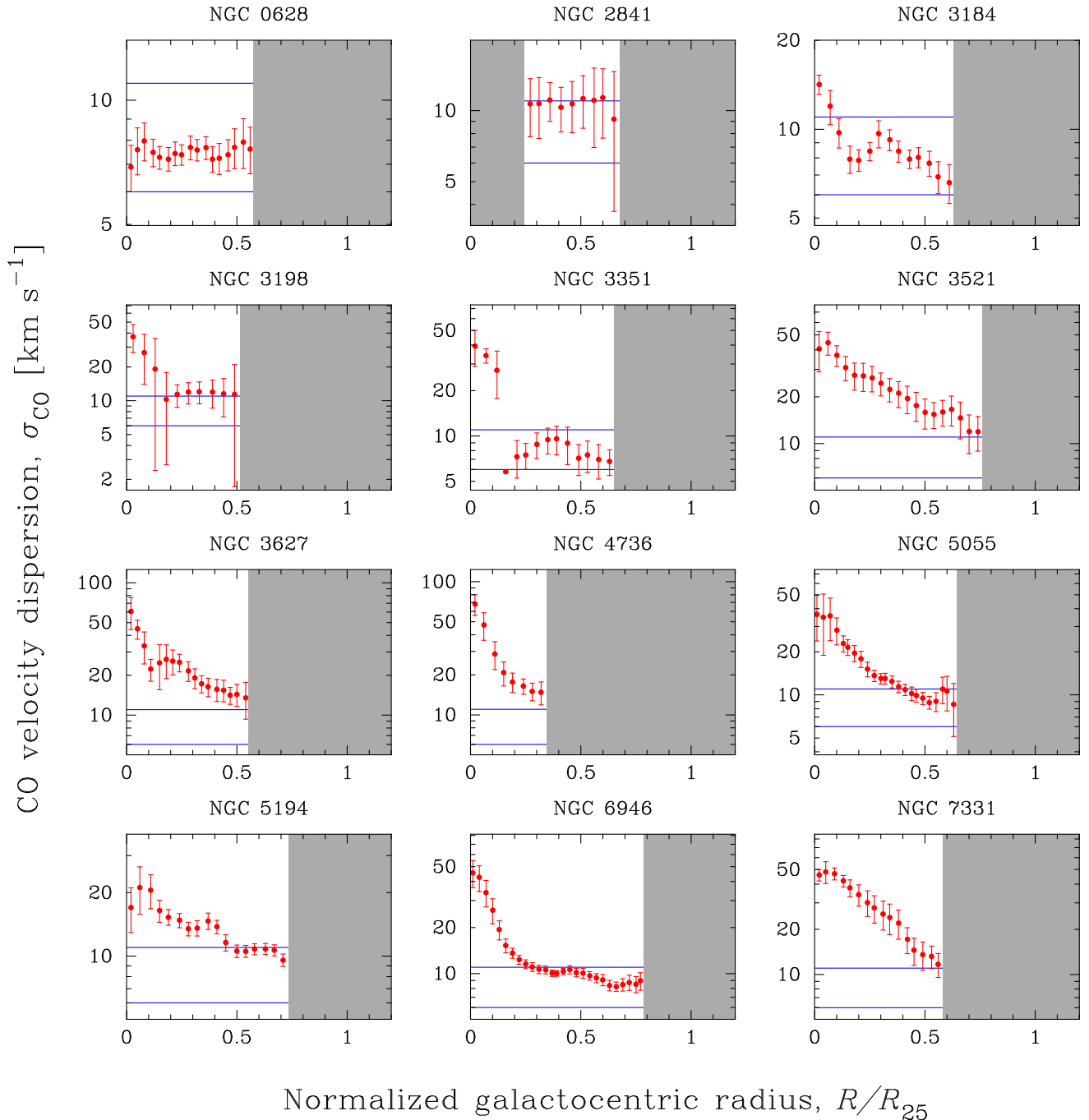


Figure 1. Radial profiles of the 1D velocity dispersion of molecular gas for each spiral of the sample, with the galactocentric distance measured in units of the optical radius. In the shaded regions, the total surface density of molecular gas is $\Sigma_{\text{CO}} \leq 1.0 M_{\odot} \text{pc}^{-2}$ (L08).

number of pixels in the ring where there are detections divided by the number of pixels per resolution element). Here again our approach is consistent with that followed by L08 (M16 averaged azimuthally over 13-arcsec rings where both CO and H I have filling factors larger than 10 per cent).

Figs 1 and 2 show $\sigma_{\text{CO}}(R)$ and $\sigma_{\text{H I}}(R)$ for each spiral of our sample, as well as representative values of σ_{CO} and $\sigma_{\text{H I}}$ motivated/used in previous stability analyses: $\sigma_{\text{CO}} = 6 \text{ km s}^{-1}$ (e.g. Kennicutt 1989; Wilson et al. 2011; Romeo & Falstad 2013; Hallenbeck et al. 2016), $\sigma_{\text{CO}} = 11 \text{ km s}^{-1}$ (L08) and $\sigma_{\text{H I}} = 11 \text{ km s}^{-1}$ (e.g. L08; Romeo & Falstad 2013; Hallenbeck et al. 2016). Also shown, as

shaded regions, are the radial ranges where $\Sigma_{\text{CO}} \leq 1.0 M_{\odot} \text{pc}^{-2}$ and $\Sigma_{\text{H I}} \leq 1.0 M_{\odot} \text{pc}^{-2}$, i.e. where the CO and H I fluxes approach the detection limit of the HERACLES and THINGS surveys ($1.0 M_{\odot} \text{pc}^{-2}$ is the working sensitivity adopted by L08). CO and H I data points close to the shaded radial ranges, and H I data points close to galaxy centres, are subject to significant systematic uncertainties. This is true not only for our $\sigma_{\text{CO}}(R)$ and $\sigma_{\text{H I}}(R)$, but also for L08's $\Sigma_{\text{CO}}(R)$ and $\Sigma_{\text{H I}}(R)$. Figs 1 and 2 illustrate that $\sigma_{\text{CO}}(R)$ and $\sigma_{\text{H I}}(R)$ rise towards the centre in most of the galaxies. Note that this is an order-of-magnitude effect for $\sigma_{\text{CO}}(R)$ in spirals like NGC 3351, 4736, 5055 and 6946! This form of disc heating is a

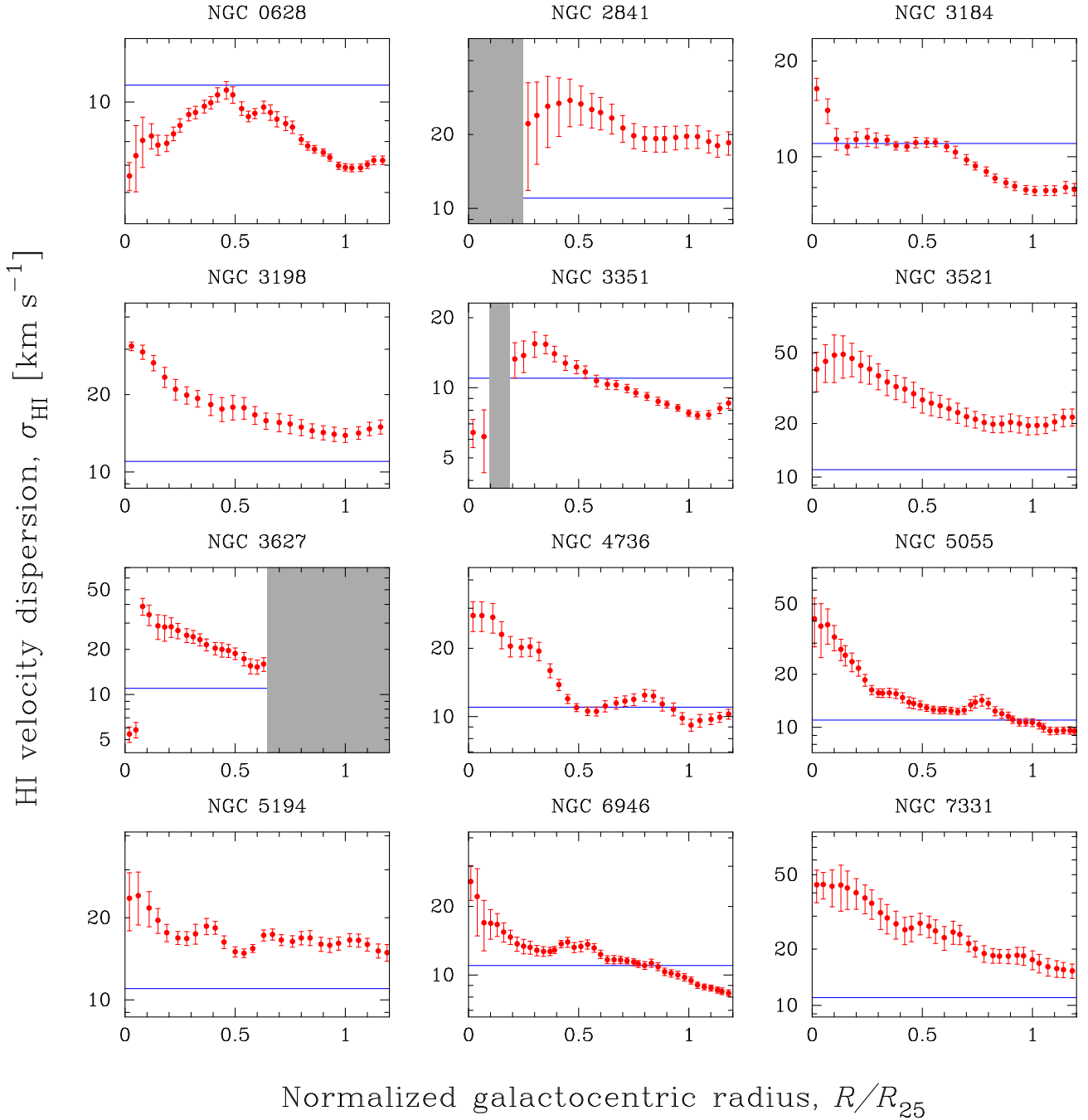


Figure 2. Radial profiles of the 1D velocity dispersion of atomic gas for each spiral of the sample, with the galactocentric distance measured in units of the optical radius. In the shaded regions, the total surface density of atomic gas is $\Sigma_{\text{HI}} \leq 1.0 M_{\odot} \text{pc}^{-2}$ (L08).

natural consequence of radial inflow and is mediated by local gravitational instabilities (e.g. Zhang 1998; Griv, Gedalin & Yuan 2002; Romeo, Horellou & Bergh 2003; Romeo, Horellou & Bergh 2004; Agertz et al. 2009; Forbes et al. 2014; Goldbaum, Krumholz & Forbes 2015, 2016; Romeo & Fathi 2015; Zhang 2016). Although there are still open questions, the basic idea behind this process is simple, and is beautifully illustrated in section 7.1 of Kormendy & Kennicutt (2004). Radial inflow increases both Σ and κ , but Σ ‘wins’ and the Toomre (1964) parameter $Q = \kappa \sigma / \pi G \Sigma$ decreases. As Q drops below a critical value of the order of unity, local gravitational instabilities set in and increase σ , thus heating the disc.

2.2 Disc-instability diagnostics

We use two disc-instability diagnostics derived by Romeo & Falstad (2013):

(i) The first diagnostic is a simple and accurate approximation for the Q stability parameter in multicomponent and realistically thick discs:

$$\frac{1}{Q_N} = \sum_{i=1}^N \frac{W_i}{T_i Q_i}, \quad (2)$$

where N is the number of gas and/or stellar components, $Q_i = \kappa\sigma_i/\pi G\Sigma_i$ is the Toomre parameter of component i (remember that σ denotes the radial velocity dispersion), T_i is a factor that encapsulates the stabilizing effect of disc thickness for the whole range of velocity dispersion anisotropy (σ_z/σ_R) observed in galactic discs and W_i is a weight factor. T_i and W_i are given by

$$T_i = \begin{cases} 1 + 0.6 \left(\frac{\sigma_z}{\sigma_R} \right)_i^2 & \text{if } 0 \leq (\sigma_z/\sigma_R)_i \leq 0.5, \\ 0.8 + 0.7 \left(\frac{\sigma_z}{\sigma_R} \right)_i & \text{if } 0.5 \leq (\sigma_z/\sigma_R)_i \leq 1, \end{cases} \quad (3)$$

$$W_i = \frac{2\sigma_m\sigma_i}{\sigma_m^2 + \sigma_i^2}, \quad (4)$$

where m is the component with smallest TQ :

$$T_m Q_m = \min\{T_i Q_i\}. \quad (5)$$

(ii) The second diagnostic is a corresponding approximation for the characteristic instability scale, i.e. the perturbation wavelength at which the disc becomes locally unstable as Q_N drops below unity:

$$\lambda_N = 2\pi \frac{\sigma_m}{\kappa}, \quad (6)$$

where m is defined by equation (5).

This set of equations tells us that the values of Q_N and λ_N are controlled by the component with smallest TQ . This is the component that drives disc instabilities: $Q_N \sim T_m Q_m$ ($W_m = 1$). All other components have less weight because their contributions are weakened by factors $W_i < 1$; the more σ_i differs from σ_m , the smaller is W_i . Note that while $Q_N > 1$ ensures stability against axisymmetric perturbations, larger values of Q_N ($\gtrsim 2-3$) are required to stabilize the disc against non-axisymmetric perturbations (e.g. Griv & Gedalin 2012) and gas dissipation (Elmegreen 2011).

To compute the radial profiles of Q_3 and λ_3 ($N = 3$ in our case), we need to specify $T_{CO}(R)$, $T_{H_1}(R)$ and $T_*(R)$; the radial profiles of all basic quantities have already been specified (see Section 2). Following Romeo & Falstad (2013), we adopt constant $(\sigma_z/\sigma_R)_{CO} = (\sigma_z/\sigma_R)_{H_1} = 1$, as is natural for collisional components, and a constant $(\sigma_z/\sigma_R)_* = 0.6$, as was assumed by L08. Hence, $T_{CO} = T_{H_1} = 1.5$, and $T_* = 1.22$.

3 RESULTS

Fig. 3 shows the three-component Q stability parameter as a function of galactocentric distance for our sample of spirals. Also shown is the local median of Q_3 , $Q_{\text{med}}(R)$, computed by binning the data in 12 rings of width $0.1 R/R_{25}$. This apparently simple plot encloses two layers of information. The first layer is well known: The stability level of nearby star-forming spirals is, on average, remarkably flat and well above unity (e.g. L08; Romeo & Falstad 2013). In fact, the local median of Q_3 varies within the range $2 \lesssim Q_{\text{med}}(R) \lesssim 3$, and globally $Q_3 = 2.2 \pm 0.6$ (global median $\pm 1\sigma$ scatter). Remember that $Q_3 > 1$ ensures stability against axisymmetric perturbations, while larger values of Q_3 ($> Q_{\text{crit}}$) are required to stabilize the disc against non-axisymmetric perturbations. Unfortunately, there is still no general consensus about the value of Q_{crit} . For example, Griv & Gedalin (2012) found that the classical estimate $Q_{\text{crit}} \approx 2$ is an absolute upper limit on the critical stability level. Elmegreen (2011) showed that gas dissipation has a similar destabilizing effect, and estimated that $Q_{\text{crit}} \approx 2-3$. If one assumes this local stability

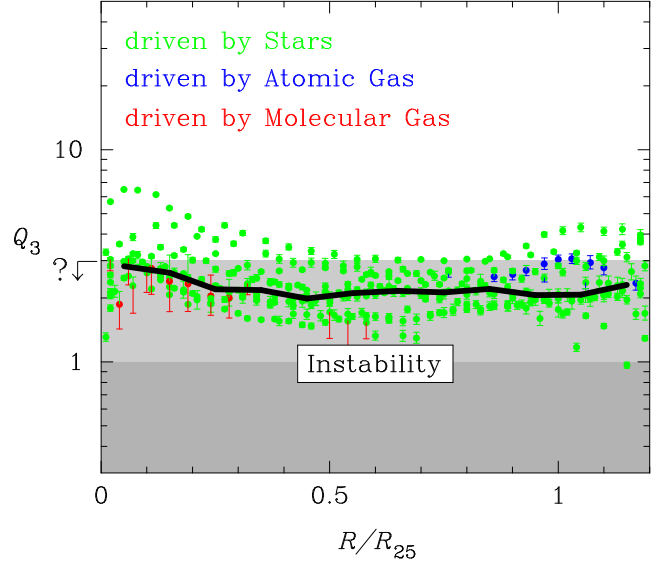


Figure 3. Radial profiles of the three-component Q stability parameter for the whole sample of spirals, with the galactocentric distance measured in units of the optical radius. Also shown is the local median of Q_3 . Note that while $Q_3 > 1$ ensures stability against axisymmetric perturbations, larger values of Q_3 ($\gtrsim 2-3$) are required to stabilize the disc against non-axisymmetric perturbations and gas dissipation. The precise value of the critical stability level is still questioned (see Section 3). The data are colour-coded so as to show whether disc instabilities are driven by stars, atomic or molecular gas.

threshold, then nearby star-forming spirals are close to marginal instability or unstable, given that 52 per cent of the data fall within the range $2 \leq Q_3 \leq 3$ and that $Q_3 < 2$ in 30 per cent of the cases. The second layer of information is deeper and can be extracted only by using the Romeo–Falstad disc instability diagnostics. It concerns the component that drives gravitational instability, which has important dynamical implications, as we discuss below.

Fig. 4 is the *key plot* of our paper. It illustrates that using observed radial profiles of σ_{CO} , rather than observationally motivated values of σ_{CO} , has a strong impact on the inferred scale of gravitational instabilities in nearby star-forming spirals. Let us first see what a $\sigma_{CO} = 6 \text{ km s}^{-1}$ analysis predicts. Remember that this is the value of σ_{CO} motivated by Kennicutt (1989), Martin & Kennicutt (2001) and Wilson et al. (2011), among others, and the one used by Romeo & Falstad (2013). The left-hand panel of Fig. 4 shows the three-component characteristic instability scale as a function of galactocentric distance for our sample of spirals. The colour coding tells us which component drives gravitational instability: molecular gas, atomic gas or stars. Note (i) that disc instabilities are driven by the stars in 82 per cent of the cases, but molecular gas is nevertheless an important driver of gravitational instability in the inner disc; (ii) that the distribution of $\lambda_3(R)$ is bimodal for $R \lesssim 0.5 R_{25}$; and (iii) that there is an order-of-magnitude gap in λ_3 between regimes driven by the molecular gas (a few 100 pc) and regimes driven by the stars (a few kpc). What does our analysis predict instead? See the right-hand panel of Fig. 4. The rise of $\sigma_{CO}(R)$ towards the centre results in a paradigm shift. Inner disc instabilities are now entirely driven by the stars at kpc scales ($\lambda_3 = 5.9 \pm 2.3 \text{ kpc}$), with two notable exceptions: the inner discs of NGC 5194 and NGC 6946 (2 per cent of the data). These are the sample galaxies with highest surface density of molecular gas averaged over the inner disc ($\langle \Sigma_{CO} \rangle \approx 150 M_{\odot} \text{ pc}^{-2}$ for $R \leq 0.3 R_{25}$), and highest star formation

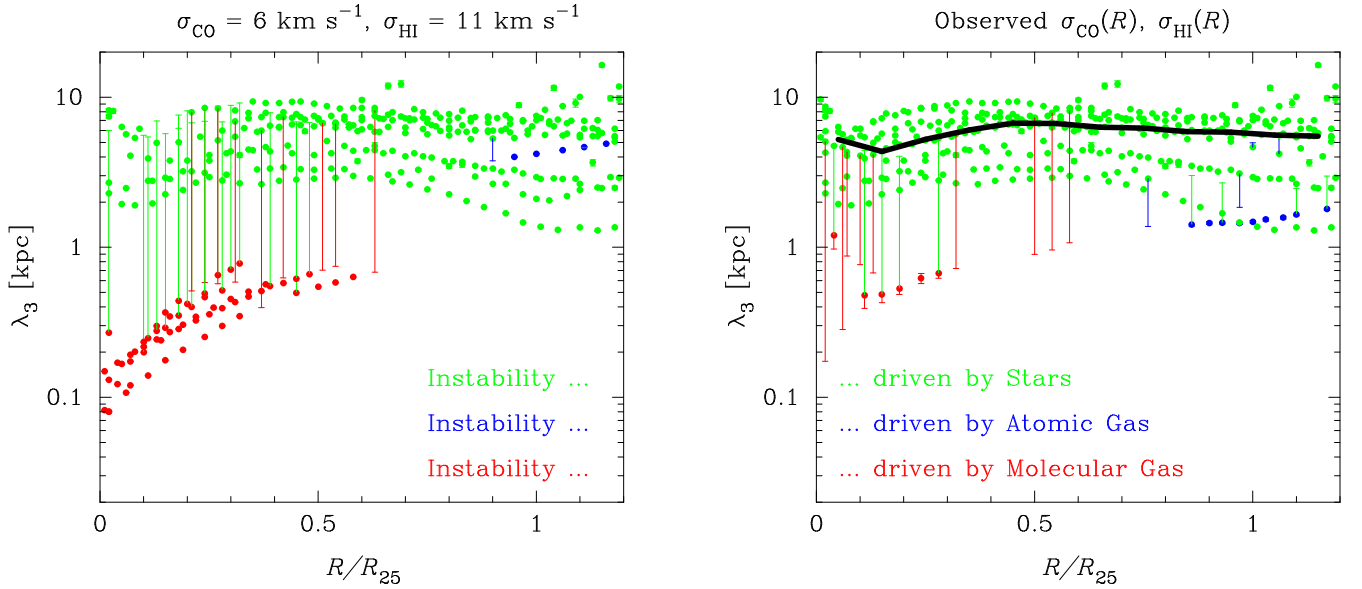


Figure 4. Radial profiles of the three-component characteristic instability scale for the whole sample of spirals, with the galactocentric distance measured in units of the optical radius. Left-hand panel: the result of using observationally motivated values of σ_{CO} and σ_{HI} , as in Romeo & Falstad (2013). Right-hand panel: the result of using our observed radial profiles of σ_{CO} and σ_{HI} ; also shown is the local median of λ_3 . The data are colour-coded so as to show whether disc instabilities are driven by stars, atomic or molecular gas.

rate ($\text{SFR} \gtrsim 3 M_{\odot} \text{yr}^{-1}$; see table 4 of L08 or table 1 of Walter et al. 2008). These are also active galaxies, where molecular gas plays a key role as fuel in the activity process (e.g. Krips et al. 2008). Fig. 4 also shows that atomic gas plays a negligible role as driver of gravitational instability up to the edge of the optical disc, regardless of whether one uses $\sigma_{\text{HI}} = 11 \text{ km s}^{-1}$ (L08; Romeo & Falstad 2013) or our observed $\sigma_{\text{HI}}(R)$.

Can star-driven instabilities lead to local gravitational collapse/fragmentation in the molecular gas? To answer this question, we should understand in more detail how molecular gas and stars contribute to disc instabilities. This important piece of information is illustrated in Fig. 5. Consider a two-component disc of molecular gas and stars, and perturb it with axisymmetric waves of frequency ω and wavenumber k . The response of the disc is basically described by the Jog & Solomon (1984a) dispersion relation, $\omega^2(k)$. Inside the ‘two-phase region’ shown in Fig. 5, $\omega^2(k)$ has two distinct minima (Bertin & Romeo 1988; Romeo & Wiegert 2011). In the ‘gaseous phase’, the minimum at short wavelengths ($\lambda = 2\pi/k$) is lower than the other one and molecular gas will drive the onset of gravitational instability. Vice versa, in the ‘stellar phase’, the long-wavelength minimum is lower and stars will drive instability. The shape and size of this region are only moderately affected by disc thickness (Romeo & Wiegert 2011), gas turbulence (Hoffmann & Romeo 2012) or the fact that the stellar component is collisionless (Romeo & Falstad 2013). In the rest of the parameter plane, $\omega^2(k)$ has a single minimum, where the dynamical responses of the two components are strongly coupled. This means that any instability driven by one of the components will also perturb and destabilize the other. In particular, star-driven instabilities will lead to local gravitational collapse/fragmentation in the molecular gas. This is clearly the case for almost the entire galaxy sample, as almost the entire data set falls outside the two-phase region. The inner discs of NGC 5194 and 6946 are again exceptions to the general rule. But instabilities in such discs are driven by the molecular gas (see discussion of Fig. 4), so they will naturally lead to its collapse or fragmentation.

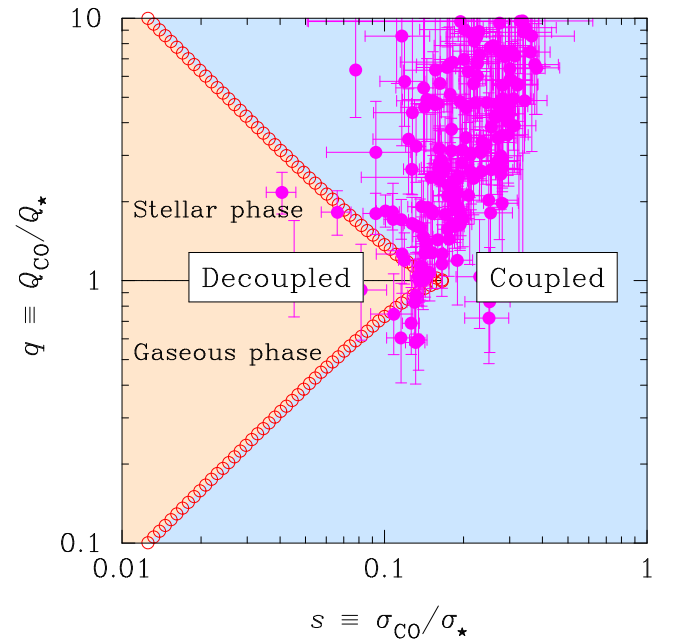


Figure 5. The parameter plane of two-component disc instabilities populated by the galaxy data. Here σ_{CO} and σ_{\star} are the radial velocity dispersions of molecular gas and stars, and Q_{CO} and Q_{\star} are their Toomre parameters. Outside the ‘two-phase region’, the responses of the two components to perturbations are coupled. So star-driven instabilities can also lead to local gravitational collapse/fragmentation in the molecular gas.

4 DISCUSSION

Are NGC 5194 and 6946 true outliers? The condition that disc instabilities are driven by stars, rather than molecular gas, is

$$T_{\star} Q_{\star} < T_{\text{CO}} Q_{\text{CO}} \implies T_{\star} \sigma_{\star} / \Sigma_{\star} < T_{\text{CO}} \sigma_{\text{CO}} / \Sigma_{\text{CO}} \quad (7)$$

(see Section 2.2 and remember that Σ_{CO} denotes the total surface density of molecular gas, helium included). As pointed out in Section 3, this condition is not fulfilled by the inner discs of NGC 5194 and 6946. On the other hand, it turns out that if $T_*\sigma_*/\Sigma_*$ were 29 per cent smaller, or if $T_{\text{CO}}\sigma_{\text{CO}}/\Sigma_{\text{CO}}$ were 41 per cent larger ($1/0.71 = 1.41$), then gravitational instabilities in such discs would be driven by the stars, as in the rest of the galaxy sample. Can systematic uncertainties account for that? Let us discuss this point below.

It is well known that the surface densities of molecular gas and stars are subject to significant systematic uncertainties via the adopted CO-to-H₂ conversion factor, X_{CO} , and stellar mass-to-light ratio, Υ_* (see e.g. Binney & Merrifield 1998). L08 adopted $X_{\text{CO}} = 2 \times 10^{20} \text{ cm}^{-2} (\text{K km s}^{-1})^{-1}$. This is the standard value recommended by Bolatto, Wolfire & Leroy (2013) for the discs of normal solar-metallicity galaxies, and has an uncertainty of ± 0.3 dex (a factor of 2). Sandstrom et al. (2013) carried out one of the most comprehensive extragalactic study of X_{CO} to date, and found an average value of X_{CO} that is 30 per cent smaller than the standard one: $(X_{\text{CO}}) = 1.4 \times 10^{20} \text{ cm}^{-2} (\text{K km s}^{-1})^{-1}$, again with an uncertainty of ± 0.3 dex. This value of X_{CO} is small enough to move the inner discs of NGC 5194 and 6946 into star-driven instability regimes! Concerning the stellar mass-to-light ratio, L08 adopted $\Upsilon_*^K = 0.5 M_{\odot}/L_{\odot,K}$. This is near the mean K -band M/L ratio expected for these galaxies (Bell et al. 2003), and has an uncertainty of ± 0.1 – 0.2 dex (a factor of 1.3–1.6). A value of $\Upsilon_*^K = 0.7 M_{\odot}/L_{\odot,K}$ would be large enough to ‘normalize’ NGC 5194 and 6946, and still be within the uncertainty range.

Another source of significant systematic uncertainty is the stellar radial velocity dispersion. In fact, in contrast to our $\sigma_{\text{CO}}(R)$, the radial profiles of σ_* derived by L08 are not based on observations, but on a simple model that relates σ_* to the surface density and scalelength of the stellar disc (see appendix B.3 of L08). To the best of our knowledge, stellar velocity dispersions have been measured only in three galaxies of the sample: NGC 628 (Ganda et al. 2006; Herrmann & Ciardullo 2009), NGC 3198 (Bottema 1988, 1993) and NGC 4736 (Herrmann & Ciardullo 2009). To estimate the accuracy of L08’s model, we consider the radial profiles of σ_{z*} derived by Herrmann & Ciardullo (2009) for NGC 628 and 4736, and convert σ_{z*} into σ_* using the best-fitting model of Gerssen & Shapiro Griffin (2012), which relates $(\sigma_z/\sigma_R)_*$ to galaxy type (see their fig. 4). Fig. 6 shows that L08’s model is accurate to within a factor of 2 except in the innermost/outermost regions of the stellar disc, where this model can overestimate/underestimate the observed $\sigma_*(R)$ by a larger factor. Our $\sigma_{\text{CO}}(R)$ is less uncertain. The main source of systematic uncertainty is beam smearing, which is greatest in the central regions of highly inclined galaxies (e.g. Teuben 2002; Caldú-Primo et al. 2013). However, beam smearing can increase the velocity dispersion by at most a factor of 1.2 at $R = 0.2 R_{25}$ for galaxies with 30° inclination, 1.5 for 60° and 1.8 for 80° , with these factors decreasing quickly towards unity at larger radii (Caldú-Primo et al. 2013).

The bottom line is that systematic uncertainties in Σ_{CO} or in Σ_* and σ_* can account for a significant increase in $T_{\text{CO}}Q_{\text{CO}}$ or decrease in T_*Q_* , and thus move the inner discs of NGC 5194 and 6946 into star-driven instability regimes. This is not surprising. Stars are the primary driver of gravitational instabilities even in the inner disc of NGC 1068, a powerful nearby Seyfert+starburst galaxy (Romeo & Fathi 2016).

Finally, the result that molecular gas plays a secondary role in disc instabilities (at low redshift) is based on the spatial resolution of current extragalactic surveys: BIMA SONG, HERACLES,

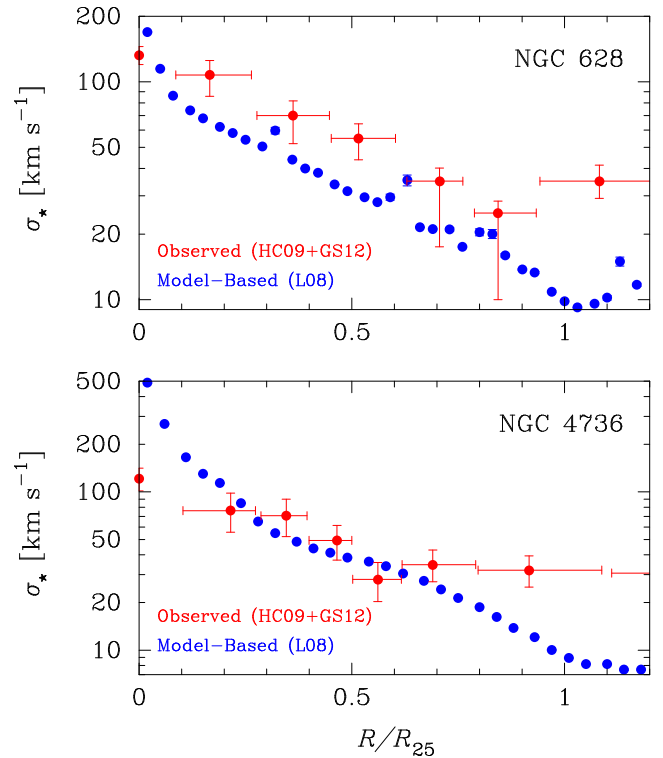


Figure 6. Observed versus model-based radial profiles of the stellar radial velocity dispersion for two spirals of the sample, with the galactocentric distance measured in units of the optical radius.

SINGS and THINGS. At scales smaller than a few hundred pc, interstellar turbulence excites two non-classical instability regimes where molecular gas plays a primary role. Such regimes stretch from galactic-scale Toomre instability to clump-scale (3D) Jeans instability, and may be one of the missing links between disc instabilities and star formation. Such regimes are illustrated in fig. 1 of Romeo et al. (2010); *the stability map of turbulence* (see also Hoffmann & Romeo 2012; Romeo & Agertz 2014; Agertz et al. 2015).

5 CONCLUSIONS

In this paper, we have analysed the stability of a sample of 12 nearby star-forming spirals using the Romeo–Falstad Q stability parameter, Q_N , and characteristic instability scale, λ_N , for $N = 3$ disc components: molecular gas, atomic gas and stars. The most novel feature of our analysis is that we have made use of observed radial profiles of the CO and H I velocity dispersions, rather than observationally motivated values of σ_{CO} and σ_{HI} . Our major conclusions are as follows:

- (i) The CO velocity dispersion has a strong impact on the disc instability scenario, as illustrated in Fig. 4. Using the classical value $\sigma_{\text{CO}} = 6 \text{ km s}^{-1}$ motivated by Kennicutt (1989), one would infer that molecular gas plays a significant role in disc instabilities even at distances as large as half the optical radius. In particular, the characteristic instability scale would have a bimodal radial distribution with an order-of-magnitude gap between regimes driven by the molecular gas ($\lambda_3 \approx 80$ – 800 pc) and regimes driven by the stars ($\lambda_3 \approx 2$ – 10 kpc). Using, instead, our radial profiles of σ_{CO} results in disc instabilities that are almost entirely driven by the stars. The characteristic instability scale has median value $\lambda_3 = 5.9$ kpc and 1σ scatter $\Delta \log \lambda_3 = 0.16$ dex (a factor of 1.4); 2 per cent of the

data are ‘outliers’, which systematic uncertainties can move into star-driven regimes.

(ii) In contrast to the characteristic instability scale, the Q stability parameter is robust against radial variations in both σ_{HI} and σ_{CO} . On average, its radial profile remains remarkably flat and well above unity, but near or below the approximate threshold for stability against local, non-axisymmetric, linear perturbations and gas dissipation ($Q_3 \approx 2-3$). Specifically, the Q stability parameter has median value $Q_3 = 2.2$ and 1σ scatter $\Delta \log Q_3 = 0.11$ dex (a factor of 1.3); 52 per cent of the data fall within the range $2 \leq Q_3 \leq 3$, and $Q_3 < 2$ in 30 per cent of the cases.

(iii) The conclusion that stars are the primary driver of disc instabilities in nearby star-forming spirals requires two further clarifications. First, in the linear phase of the disc instability process, stars are strongly coupled to molecular gas, as shown in Fig. 5. This means that any instability driven by the stars will also perturb and destabilize molecular gas, and thus lead to local gravitational collapse/fragmentation. Secondly, the fact that stars set the initial conditions for gravitational instability is true at the spatial resolution of current extragalactic surveys: BIMA SONG, HERACLES, SINGS and THINGS. At scales smaller than ~ 100 pc, interstellar turbulence opens new instability channels in which molecular gas plays a primary role (e.g. Romeo et al. 2010).

ACKNOWLEDGEMENTS

ABR dedicates this paper to his father Francesco: in your memory, with infinite love and sorrow. This work made use of data from the following surveys: BIMA SONG (Helfer et al. 2003), HERACLES (Leroy et al. 2009), SINGS (Kennicutt et al. 2003) and THINGS (Walter et al. 2008). This work also made use of radial profiles derived by Leroy et al. (2008) and Herrmann & Ciardullo (2009). We are very grateful to Oscar Agertz, Kim Herrmann and Andreas Schrubba for useful discussions. We are also grateful to an anonymous referee for constructive comments and suggestions, and for encouraging future work on the topic. KMM gratefully acknowledges support from the Square Kilometre Array South Africa (SKA-SA).

REFERENCES

Agertz O., Lake G., Teyssier R., Moore B., Mayer L., Romeo A. B., 2009, *MNRAS*, 392, 294
 Agertz O., Romeo A. B., Grisdale K., 2015, *MNRAS*, 449, 2156
 Athanassoula E., 2013, in Falcón-Barroso J., Knapen J. H., eds, *Secular Evolution of Galaxies*. Cambridge Univ. Press, Cambridge, p. 305
 Bell E. F., McIntosh D. H., Katz N., Weinberg M. D., 2003, *ApJS*, 149, 289
 Bertin G., 2014, *Dynamics of Galaxies*. Cambridge Univ. Press, Cambridge
 Bertin G., Romeo A. B., 1988, *A&A*, 195, 105
 Binney J., Merrifield M., 1998, *Galactic Astronomy*. Princeton Univ. Press, Princeton, NJ
 Bolatto A. D., Wolfire M., Leroy A. K., 2013, *ARA&A*, 51, 207
 Bottema R., 1988, *A&A*, 197, 105
 Bottema R., 1993, *A&A*, 275, 16
 Caldú-Primo A., Schrubba A., Walter F., Leroy A., Sandstrom K., de Blok W. J. G., Ianjamasimanana R., Mogotsi K. M., 2013, *AJ*, 146, 150
 Dobbs C. L. et al., 2014, in Beuther H., Klessen R. S., Dullemond C. P., Henning T., eds, *Protostars and Planets VI*. Univ. Arizona Press, Tucson, AZ, p. 3
 Elmegreen B. G., 1995, *MNRAS*, 275, 944
 Elmegreen B. G., 1996, in Block D. L., Greenberg J. M., eds, *New Extragalactic Perspectives in the New South Africa*. Kluwer, Dordrecht, p. 467
 Elmegreen B. G., 2011, *ApJ*, 737, 10

Elmegreen B. G., 2012, in Tuffs R. J., Popescu C. C., eds, *Proc. IAU Symp.* 284, *The Spectral Energy Distribution of Galaxies*. Cambridge Univ. Press, Cambridge, p. 317
 Elmegreen B. G., Scalo J., 2004, *ARA&A*, 42, 211
 Fathi K. et al., 2015, *ApJ*, 806, L34
 Ferguson A. M. N., Wyse R. F. G., Gallagher J. S., Hunter D. A., 1998, *ApJ*, 506, L19
 Fiacconi D., Mayer L., Madau P., Lupi A., Dotti M., Haardt F., 2017, *MNRAS*, 467, 4080
 Forbes J. C., Krumholz M. R., Burkert A., Dekel A., 2014, *MNRAS*, 438, 1552
 Ganda K., Falcón-Barroso J., Peletier R. F., Cappellari M., Emsellem E., McDermid R. M., de Zeeuw P. T., Carollo C. M., 2006, *MNRAS*, 367, 46
 Genzel R. et al., 2014, *ApJ*, 785, 75
 Gerssen J., Shapiro Griffin K., 2012, *MNRAS*, 423, 2726
 Goldbaum N. J., Krumholz M. R., Forbes J. C., 2015, *ApJ*, 814, 131
 Goldbaum N. J., Krumholz M. R., Forbes J. C., 2016, *ApJ*, 827, 28
 Goldreich P., Lynden-Bell D., 1965a, *MNRAS*, 130, 97
 Goldreich P., Lynden-Bell D., 1965b, *MNRAS*, 130, 125
 Grisdale K., Agertz O., Romeo A. B., Renaud F., Read J. I., 2017, *MNRAS*, 466, 1093
 Griv E., Gedalin M., 2012, *MNRAS*, 422, 600
 Griv E., Gedalin M., Yuan C., 2002, *A&A*, 383, 338
 Hallenbeck G. et al., 2016, *AJ*, 152, 225
 Helfer T. T., Thornley M. D., Regan M. W., Wong T., Sheth K., Vogel S. N., Blitz L., Bock D. C.-J., 2003, *ApJS*, 145, 259
 Hennebelle P., Falgarone E., 2012, *A&AR*, 20, 55
 Herrmann K. A., Ciardullo R., 2009, *ApJ*, 705, 1686
 Hoffmann V., Romeo A. B., 2012, *MNRAS*, 425, 1511
 Ianjamasimanana R., de Blok W. J. G., Walter F., Heald G. H., Caldú-Primo A., Jarrett T. H., 2015, *AJ*, 150, 47
 Ianjamasimanana R., de Blok W. J. G., Heald G. H., 2017, *AJ*, 153, 213
 Inoue S., Dekel A., Mandelker N., Ceverino D., Bournaud F., Primack J., 2016, *MNRAS*, 456, 2052
 Jog C. J., 1996, *MNRAS*, 278, 209
 Jog C. J., Solomon P. M., 1984a, *ApJ*, 276, 114
 Jog C. J., Solomon P. M., 1984b, *ApJ*, 276, 127
 Kennicutt R. C., Jr, 1989, *ApJ*, 344, 685
 Kennicutt R. C., Jr, et al., 2003, *PASP*, 115, 928
 Kim W.-T., Ostriker E. C., 2007, *ApJ*, 660, 1232
 Kormendy J., Kennicutt R. C., Jr, 2004, *ARA&A*, 42, 603
 Kraljic K., Renaud F., Bournaud F., Combes F., Elmegreen B., Emsellem E., Teyssier R., 2014, *ApJ*, 784, 112
 Krips M., Neri R., García-Burillo S., Martín S., Combes F., Graciá-Carpio J., Eckart A., 2008, *ApJ*, 677, 262
 Kruijssen J. M. D., 2014, *Class. Quantum Gravity*, 31, 244006
 Krumholz M. R., McKee C. F., 2005, *ApJ*, 630, 250
 Leroy A. K., Walter F., Brinks E., Bigiel F., de Blok W. J. G., Madore B., Thornley M. D., 2008, *AJ*, 136, 2782 (L08)
 Leroy A. K. et al., 2009, *AJ*, 137, 4670
 Lin C. C., Shu F. H., 1966, *Proc. Natl. Acad. Sci. USA*, 55, 229
 Martin C. L., Kennicutt R. C., Jr, 2001, *ApJ*, 555, 301
 Mogotsi K. M., de Blok W. J. G., Caldú-Primo A., Walter F., Ianjamasimanana R., Leroy A. K., 2016, *AJ*, 151, 15 (M16)
 Rafikov R. R., 2001, *MNRAS*, 323, 445
 Romeo A. B., 1985, *Stabilità di Sistemi Stellari in Presenza di Gas: Fenomeni Collettivi in Sistemi Autogravitanti a Due Componenti*. Tesi di Laurea, University of Pisa and Scuola Normale Superiore, Pisa
 Romeo A. B., 1990, PhD thesis, SISSA
 Romeo A. B., 1992, *MNRAS*, 256, 307
 Romeo A. B., 1994, *A&A*, 286, 799
 Romeo A. B., Agertz O., 2014, *MNRAS*, 442, 1230
 Romeo A. B., Falstad N., 2013, *MNRAS*, 433, 1389
 Romeo A. B., Fathi K., 2015, *MNRAS*, 451, 3107
 Romeo A. B., Fathi K., 2016, *MNRAS*, 460, 2360
 Romeo A. B., Wiegert J., 2011, *MNRAS*, 416, 1191
 Romeo A. B., Horellou C., Bergh J., 2003, *MNRAS*, 342, 337

- Romeo A. B., Horellou C., Bergh J., 2004, MNRAS, 354, 1208
Romeo A. B., Burkert A., Agertz O., 2010, MNRAS, 407, 1223
Safronov V. S., 1960, Ann. Astrophys., 23, 979
Salim D. M., Federrath C., Kewley L. J., 2015, ApJ, 806, L36
Sandstrom K. M. et al., 2013, ApJ, 777, 5
Sellwood J. A., 2014, Rev. Mod. Phys., 86, 1
Semenov V. A., Kravtsov A. V., Gnedin N. Y., 2016, ApJ, 826, 200
Shadmehri M., Khajenabi F., 2012, MNRAS, 421, 841
Shlosman I., Frank J., Begelman M. C., 1989, Nature, 338, 45
Tamburro D., Rix H.-W., Leroy A. K., Mac Low M.-M., Walter F., Kennicutt R. C., Brinks E., de Blok W. J. G., 2009, AJ, 137, 4424
Teuben P. J., 2002, in Athanassoula E., Bosma A., Mujica R., eds, ASP Conf. Ser. Vol. 275, Disks of Galaxies: Kinematics, Dynamics and Perturbations. Astron. Soc. Pac., San Francisco, p. 217
Toomre A., 1964, ApJ, 139, 1217
Walter F., Brinks E., de Blok W. J. G., Bigiel F., Kennicutt R. C., Jr, Thornley M. D., Leroy A., 2008, AJ, 136, 2563
Westfall K. B., Andersen D. R., Bershadsky M. A., Martinsson T. P. K., Swaters R. A., Verheijen M. A. W., 2014, ApJ, 785, 43
Williamson D., Martel H., Kawata D., 2016a, ApJ, 822, 91
Williamson D., Martel H., Romeo A. B., 2016b, ApJ, 831, 1
Wilson C. D. et al., 2011, MNRAS, 410, 1409
Zhang X., 1998, ApJ, 499, 93
Zhang X., 2016, Astron. Comput., 17, 86

This paper has been typeset from a $\text{\TeX}/\text{\LaTeX}$ file prepared by the author.